



Co-hydrothermal valorization of food waste: process optimization, characterization, and water decolorization application

Ayoub Abdullah Alqadami¹ · Saikh Mohammad Wabaidur¹ · Byoung-Hun Jeon² · Moonis Ali Khan¹

Received: 6 October 2022 / Revised: 22 December 2022 / Accepted: 22 December 2022 / Published online: 4 January 2023
© The Author(s), under exclusive licence to Springer-Verlag GmbH Germany, part of Springer Nature 2022

Abstract

In this study, jackfruit peel (JP) was blended into sugarcane bagasse (SB) powder during co-hydrothermal carbonization (Co-HTC) to improve the physicochemical properties of JP/SB@4:1 hydrochar for the removal of methylene blue (MB), malachite green (MG), and crystal violet (CV) dyes from aqueous solutions. JP/SB@4:1 was systematically characterized. Spectroscopic, morphological, and elemental analyses confirmed successful binding of MB, CV, and MG dyes with JP/SB@4:1 surface. Influence of various parameters such as contact time, pH, initial dyes concentration, and temperature on the adsorption process was studied. The optimized magnitudes for these parameters were found to be 480 min of contact time; pH 6.6 for MB, 7.6 for MG, and 8.3 for CV; and 328K of temperature. Non-linear kinetic and isotherm models were applied to the experimental data. Results revealed the fitting of pseudo-second-order (PSO) and Langmuir isotherm (LIM) models to experimental data, while the maximum monolayer adsorption capacities (q_m) of JP/SB@4:1 toward MB, CV, and MG were 326.79, 300.87, and 922.29 mg/g, respectively. The adsorption of dyes on JP/SB@4:1 was ascribed to electrostatic interaction, hydrogen bonding, and π - π / n - π interactions. Thermodynamics evaluation showed the feasible, spontaneous, and endothermic adsorption of the dyes.

Keywords Adsorption · Cationic dyes · Jackfruit peel · Sugarcane bagasse · Water decontamination

1 Introduction

Water contamination by dyes, pharmaceutical residues, heavy metals, and pesticides, etc., has become an environmental issue of major concern and is receiving wide attention due to the range of hazards arising therefrom. These pollutants, because of their malicious and carcinogenic nature, can be hazardous to humans and ecosystem [1]. Among organic compounds, cationic dyes such as methylene blue (MB), malachite green (MG), and crystal violet (CV) are the prominent pollutants due to their extensive

use as a coloring agent in textile, leather, paper, and pharmaceutical industries [2]. In addition, MG is also used in aquaculture industry due to its fungicidal and bactericidal efficacy. Previous studies have reported that the exposure to dyes may adversely affect human health causing anemia, skin disorders, permanent injury to the eyes, and renal blood flow [3]. Direct ingestion may trigger digestive disease and increased heart rate [4]. Therefore, for environmental and human health sustainability, the removal of dyes from the aqueous system is an urgent necessity.

Several treatment technologies, including electrochemical methods, photodegradation, membrane, coagulation, oxidation, and adsorption are commonly applied to remove dyes from wastewater. Among them, adsorption is an effective, economically efficient, and ecologically safe technique for the elimination of dyes from contaminated water. Utilization of an abundantly available solid waste biomass from different sources as a feedstock through conversion to valuables is one of the strategies set to achieve long-term environmental sustainability goals. Population increase, booming economy, and rapid urbanization have greatly accelerated the rate, amount, and quality of solid waste generation [5]. The

Ayoub Abdullah Alqadami and Saikh Mohammad Wabaidur are the authors with equal contribution.

✉ Moonis Ali Khan
mokhan@ksu.edu.sa; moonisalikhan@gmail.com

¹ Chemistry Department, College of Science, King Saud University, Riyadh 11451, Saudi Arabia

² Department of Earth Resources and Environmental Engineering, Hanyang University, Seoul 04763, Republic of Korea

production of activated carbon was favored by the utilization of solid waste namely, cow dung and chicken manure [6]. Commercially available activated carbon is a widely used carbon-based adsorbent for sequestering pollutants from water as it possesses various characteristics such as large surface area, excellent thermal stability, porous nature, and variable surface chemical composition. However, high generation cost by pyrolysis technique and regeneration cost limits its widespread applications [7]. Thus, the potential alternative for treating wastewater is hydrochar developed through hydrothermal carbonization technique (HTC).

Compared to pyrolysis, HTC has the ability to convert the wet feedstock to hydrochar with relatively high yield without prior dewatering and drying [8]. Other merits of the process are operational ease and limited pollution generation risks to the environment. In addition, hydrochar has a lower ash content, higher carbon recovery, and more surface oxygen-containing groups than the biochar produced by the pyrolysis technique [9]. Therefore, among the carbon-based adsorbents used in water decontamination, hydrochar, due to the presence of many polar functional groups such as lactone, hydroxyl, phenol, and carboxylic (developed during HTC steps [10]) is the most attractive adsorbent. Many studies have been conducted on the use of hydrochar developed from coffee husk waste [11], bamboo-derived [12], corn stover [13], olive waste [14], sewage sludge and coconut shell [15], and carboxylate-functionalized hydrochar [16] for the removal of dyes from aqueous solutions.

Jackfruit (JF, *Artocarpus heterophyllus*) is a tropical plant species belonging to the family Moraceae (originally from India) [17]. Jackfruit is the largest tree-borne fruit in the world. Usually, JF reaches 10–25 kg in weight at maturity. JF peel (JP) is one of the under-utilized waste materials and 50% of JF is composed of fibrous rind and unfertilized floral parts. JP is rich in hemicellulose, cellulose, and lignin [18]. Also, JP presents a great potential for the removal of MB from aqueous solutions [18]. Sugarcane bagasse (SB) is one of the largest agro-industrial wastes, which consists of cellulose (45%), hemicellulose (28%), and lignin (18%) [19]. Over the years, a large amount of SB has accumulated due to the expansion of sugarcane crops. Therefore, SB (based on lignin) is suitable and economically attractive for dye removal [20].

Co-hydrothermal carbonization (Co-HTC) has recently emerged as a promising thermochemical technique that can enhance the physicochemical properties of hydrochar [21]. In this study, JP was blended with SB (in varied mass ratio) during Co-HTC to improve the physicochemical properties of hydrochar for the removal of MB, CV, and MG dyes from aqueous solutions. To the best of our knowledge, the Co-HTC of JP with SB has not been reported previously. The mass ratio of JP and SB was optimized by testing the MB adsorption on developed hydrochar samples and its yield.

The optimized hydrochar sample (JP/SB@4:1) was characterized and its dyes (CV, MB, and MG) adsorption performance was tested by varying experimental parameters such as solution pH, equilibrium time, adsorbent mass, initial dyes concentration, and temperature. The adsorption kinetics, isotherm, and thermodynamics of the adsorption process were also investigated in order to optimize the process.

2 Experimental

2.1 Chemicals and reagents

Cationic dyes viz. crystal violet (CV: $C_{25}H_{30}N_3Cl$) and malachite green ($C_{23}H_{25}ClN_2$) were purchased from Sigma-Aldrich, USA, while methylene blue (MB: $C_{16}H_{18}N_3SCl$) was procured from CDH, India. Hydrochloric acid (HCl, 37%), Nitric acid (HNO_3 ; 69–71%), and sodium hydroxide (NaOH, 97.5%) were purchased from Merck, Germany. The deionized (D.I) water used during the experiments was collected by the Millipore Milli-Q water system.

2.2 Co-hydrothermal carbonization of food waste

Jackfruit peel (JP) and SB were collected from a local vegetable vendor in Riyadh. JP (through ball mill) and SB (through domestic mixer blender) were separately crushed to powder. Slurry was made by suspending JP and SB with 4:1 (w/w) ratio in 50 mL D.I water, finally transferred to 200 mL PTFE lining for hydrothermal carbonization (HTC) reaction at 498 K for 2 h under autogenous pressure condition. Thereafter, the reactor was cooled to room temperature inside an oven and a hydrochar sample (JP/SB@4:1) was collected. JP/SB@4:1 sample was washed with 100 mL of 1 M HCl solution to remove alkali and other impurities, thereafter washed to neutral pH (~7.0) with D.I water. Similar HTC conditions were applied for the preparation of other samples with varied JP and SB (w/w) ratios (Table S1). Among the developed samples, a sample (JP/SB@4:1) with the best results in the MB removal tests was selected for detailed dye adsorption studies.

2.3 Characterization

The surface morphology and elements present in the developed hydrochar samples were analyzed by high resolution-scanning electron microscopy coupled with energy dispersive X-ray analysis (HRSEM-EDX, LV-SEM; S-3500 N, Hitachi at 1.0–5.0 kV) and transmission electron microscopy (TEM, Leo 912A 8B OMEGA EF-TEM, Carl Zeiss, Germany, at 120 keV), respectively. X-ray diffraction (XRD, Smart-Lab, Rigaku) patterns of hydrochar samples were analyzed. Elemental content of pristine- and dye-saturated hydrochar

samples were analyzed by X-ray photoelectron spectroscopy (XPS, theta probe-based system, Thermo Fisher Scientific). Chemical functionalities present over the surface of pristine- and dye-saturated hydrochar samples were tested by Fourier transform infrared spectroscopy (FT-IR, Nicolet 6700, Thermo Scientific).

2.3.1 Water decolonization experiment

Batch scale adsorption experiments were carried out. 1000 mg/L MB, MG, and CV stock solutions were diluted to make adsorbate solutions of required concentrations (20, 40, 60, 80, and 100 mg/L). A series of 100 mL Erlenmeyer flasks containing 50 mL of dye solutions of the desired initial concentration (C_o) were equilibrated at room temperature (298 K) with 0.005 g of JP/SB@4:1 over a shaker at 100 rpm. At the desired contact time (t , min) or at equilibrium, solid/solution phases were separated through filtration. The residual dye concentrations were quantitatively determined by UV–visible spectrophotometer (Thermo scientific, Evolution 600, USA) at maximum absorption wavelengths (λ_{max}) of 665, 618, and 590 nm for MB, MG, and CV, respectively. The percentage adsorption (%), adsorption capacity at equilibrium (q_e , mg/g), and at contact time t (q_t , mg/g) were determined by Eqs. 1, 2, and 3, respectively as:

$$\text{Adsorption(\%)} = \frac{(C_o - C_e)}{C_o} \times 100 \quad (1)$$

$$q_e = (C_o - C_e) \times \frac{V}{m} \quad (2)$$

$$q_t = (C_o - C_t) \times \frac{V}{m} \quad (3)$$

where C_o , C_e , and C_t are the initial, equilibrium, and at any specified time t concentrations of dyes in aqueous phase (mg/L), respectively. V is the volume of adsorbate solutions (L), and m is the mass of adsorbent (g).

The influence of initial pH (pH_i) on MB, MG, and CV adsorption onto JP/SB@4:1 was examined by carrying out adsorption experiments at C_o : 25 mg/L in a series of 100 mL Erlenmeyer flasks and adsorbate solutions pH_i were adjusted between ~ 2 and 9 by adding desired amounts of 0.1 M NaOH/HCl solutions.

Contact time (t) study for dye adsorption at varied C_o : 20–100 mg/L was also carried out by varying time between 1 and 720 min. In addition, the effect of adsorbate concentrations (C_o : 20–100 mg/L) on adsorption was studied at varying temperatures (T : 298–328 K). All the adsorption experiments were performed in triplicate and average values have been reported.

3 Results and discussion

3.1 Characterization of JP/SB@4:1

Figure 1a displays the FT-IR spectra of JP/SB@4:1 and MB/MG/CV-saturated JP/SB@4:1 adsorbent and the characteristic chemical functional groups along with their respective wavenumbers are presented in Table S2. These characteristic peaks provide enough evidences to support the successful development of JP/SB@4:1. After adsorptive binding of MB, CV, and MG over JP/SB@4:1 surface some peaks were

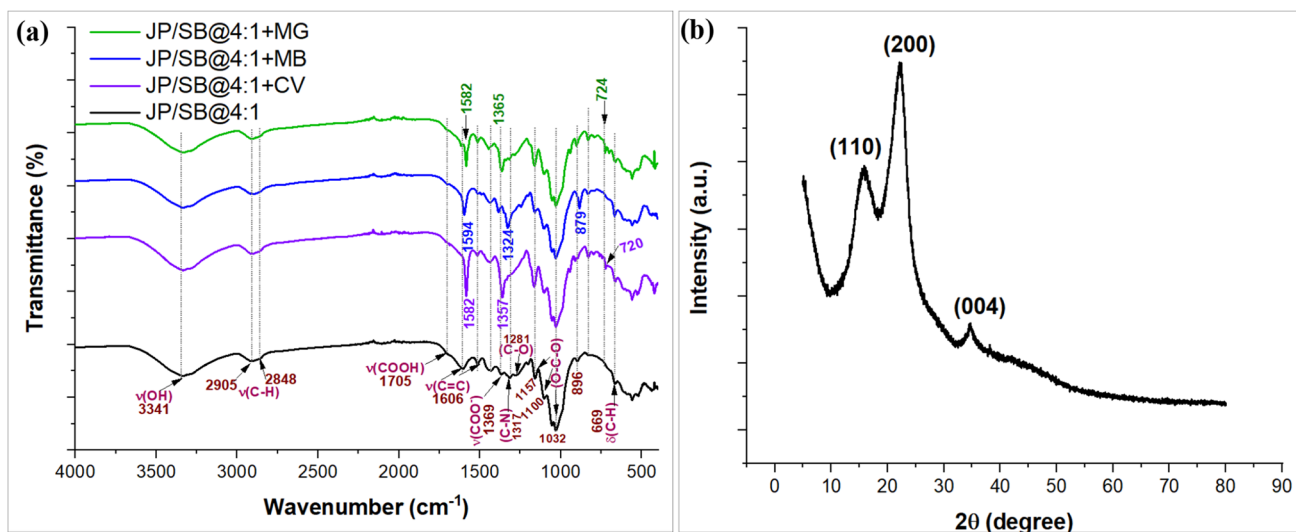


Fig. 1 FTIR spectrum (a), and XRD pattern (b) of JP/SB@4:1

appeared, increased in intensities, and/or shifted to lower wavenumbers. In detail, a peak at 1369 cm^{-1} was increased in intensity and shifted to 1357 , 1324 , and 1365 cm^{-1} after CV, MB, and MG adsorption, respectively, owing to the interaction of carboxyl group present on JP/SB@4:1 surface with $-\text{N}(\text{CH}_3)_2^+$ group of dye molecules through electrostatic interaction [23]. A peak at 3441 cm^{-1} after MG and MB adsorption was decreased in intensity, while peak intensity after CV adsorption was increased. This suggests that hydroxyl group played a vital role during the adsorption process of dye molecules through hydrogen bonding interactions [23]. A peak at 1606 cm^{-1} was increased and shifted to 1582 , 1594 , and 1582 cm^{-1} owing to the interaction of aromatic rings present over JP/SB@4:1 surface with aromatic rings of CV, MG, and MB molecules, respectively, by $\pi-\pi$ interaction. New peaks at 794 , 792 , and 791 cm^{-1} were appeared after CV, MG, and MB adsorption, respectively, which proves the successful adsorption of dyes on the JP/SB@4:1 surface [16, 23]. In addition, the peaks at 724 , and 722 cm^{-1} were noticed after MG and CV adsorption onto JP/SB@4:1 surface, respectively. These characteristic peaks provide enough evidences to support the adsorption of MB, CV, and MG over JP/SB@4:1 surface.

The XRD patterns of JP/SB@4:1 are illustrated in Fig. 1b. Three characteristic peaks were observed at $2\theta = 15.80^\circ$, 22.43° , and 34.59° , are indexed as (110), (200), and (004) planes [29]. These are the characteristic peaks for cellulose [30]. In addition, the occurrence these peaks in XRD patterns of JP/SB@4:1 affirmed that HTC temperature up to $230\text{ }^\circ\text{C}$ was safe enough to preserve cellulose content in JP/SB@4:1. This also indicates incomplete carbonization of JP/SB@4:1 [31]. The XRD results are consistent with previous studies reporting the preparation of hydrochar from bamboo [25], and rice husk [30].

The morphology and elemental analysis of pristine- and dye-saturated JP/SB@4:1 was carried out by SEM–EDX analysis as presented in Fig. S1. The elemental analysis data is displayed in Table S3. As seen in Fig. S1a, the JP/SB@4:1 surface had some cracks with both rough and smooth patches and some pores. The elemental carbon (C: 49.2%), oxygen (O: 49.9%), and nitrogen (N: 0.9%) were detected over pristine JP/SB@4:1 surface (Table S3). After CV adsorption on JP/SB@4:1, the surface becomes smooth (Fig. S1b). However, the surfaces of MB and MG loaded JP/SB@4:1 were uneven and irregular, affirming that dyes were successfully adsorbed over JP/SB@4:1 (Figs. S1c and S1d). The dye-saturated JP/SB@4:1 surface showed an increase in C and N contents, while a decrease in O content was found (Table S2). This indicates that MB, CV, and MG molecules were successfully adsorbed onto the JP/SB@4:1 surface. The C content on CV-saturated JP/SB@4:1 surface was comparatively higher than that on MG- and MB-saturated JP/SB@4:1 surfaces. This might be due to higher C content

in CV molecular structure compared to MG and MB. The elemental N content was comparatively highest on MB-saturated JP/SB@4:1. In addition, the elemental sulfur (S) was only observed on the MB-saturated JP/SB@4:1 surface.

The XPS spectra of pristine- and dye-saturated JP/SB@4:1 is illustrated in Fig. 2. According to the survey XPS spectra for JP/SB@4:1, three major peaks were observed at 284.72 , 399.97 , and 532.87 eV ascribed to C1s (76.37%), N1s (0.81%), and O1s (22.77%), respectively (Fig. 2a, Table 1). The deconvoluted C1s spectrum of pristine JP/SB@4:1 was fitted into three peaks at binding energies 284.68 , 286.39 , and 288.05 eV ascribed to C–C/C=C, C–O/C–N, and O–C=O, respectively (Fig. 2b) [32]. The high-resolution deconvoluted N1s spectrum of pristine JP/SB@4:1 presents three peaks, a peak at 399.05 eV was due to the pyridinic N bond, a peak at 400.04 eV was attributed to pyrrolic N bond, and a peak at 401.49 eV was assigned to quaternary ammonium ion (Fig. 2c) [33]. The deconvoluted O1s spectrum displayed peaks at 531.70 , 532.75 , and 533.40 eV corresponding to C–O, C=O, and O–C=O, respectively (Fig. 2d) [34]. After MB, CV, and MG adsorption, the N1s contents were increased to 1.67, 1.65, and 1.69%, respectively (Table 1). In addition, a new peak appeared at 164.55 eV attributed to the S2p in MB molecules was observed (Fig. 2e), which is in good agreement with reported literature [35]. These results suggested that MB, CV, and MG molecules were successfully adsorbed onto the JP/SB@4:1 surface.

3.2 Dye adsorption experiments

3.2.1 Effect of pH

The ability of JP/SB@4:1 to adsorb cationic dyes (MB, MG, and CV) solutions of C_0 : 25 mg/L in pH range 2.2 – 8.8 at 298 K was studied (Fig. 3a). The adsorption capacities of MB, MG, and CV dyes on JP/SB@4:1 were increased from 58 to 159 mg/g, 69.5 to 156 mg/g, and 62 to 190.9 mg/g with increase in pH from 2.5 to 6.6, 2.2 to 7.6, and 3.1 to 8.3, respectively. Further rise in pH from 6.6 to 8.8 results no visible increase MB removal efficiency, while change in MG and CV dye solution color were witnessed above pH 7.6 and 8.3, respectively. This is due to the occurrence of reaction between the dyes and OH ions [36]. The lower uptake of dyes on JP/SB@4:1 under acidic conditions was due to the protonation of functional groups ($-\text{COOH}$, $-\text{NH}_2$, $-\text{OH}$) on the JP/SB@4:1 surface [37]. These protonated sites resulted in repulsion of cationic dyes. As the pH augmented, the adsorption process was enhanced owing to deprotonation of active adsorption sites present over JP/SB@4:1 surface which results in electrostatic attraction between cationic dyes ions and negatively charged functionalities present over JP/SB@4:1 surface. Figure 3b displays the point of zero

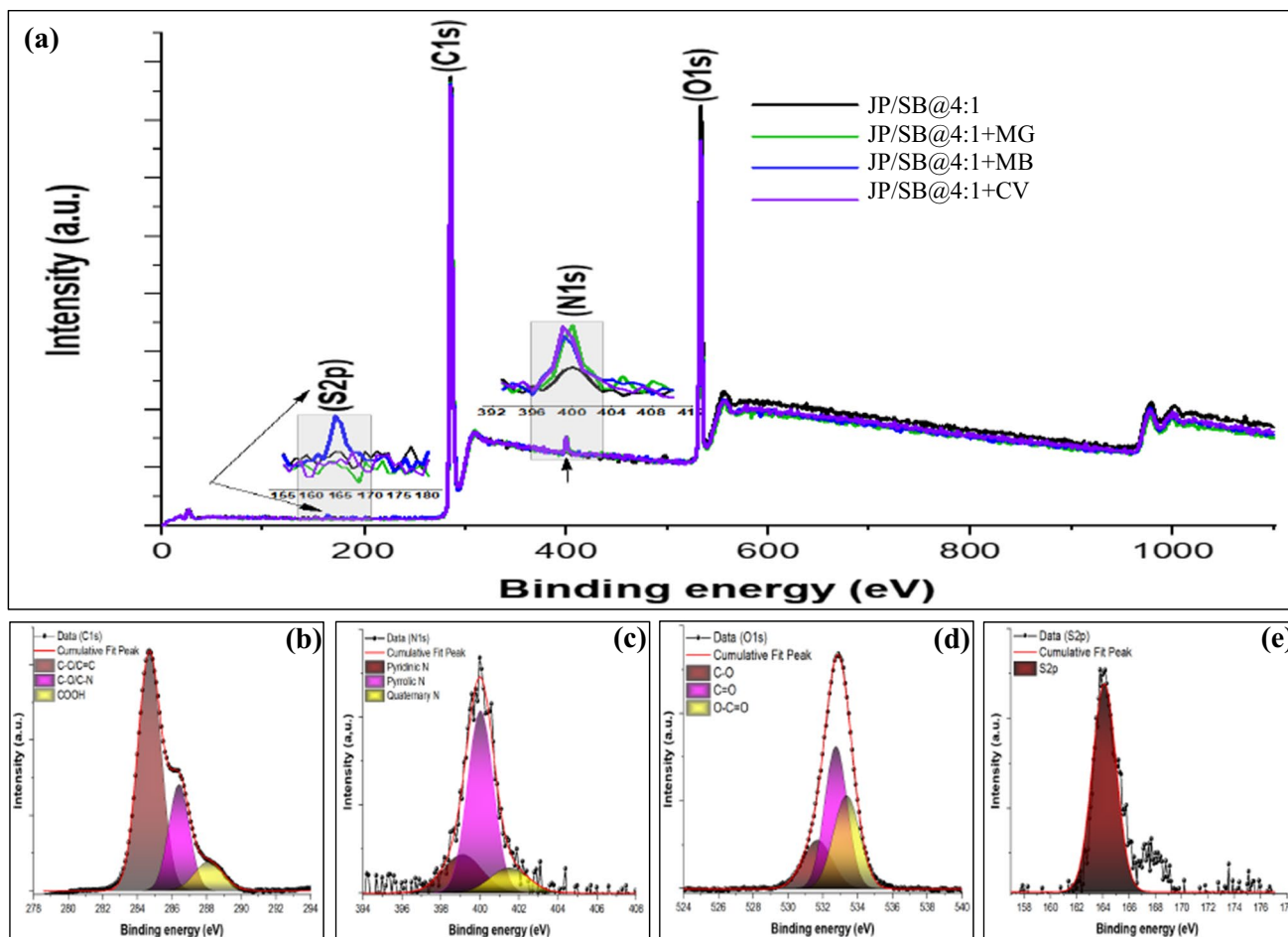


Fig. 2 Wide scan XPS spectra (a), deconvoluted C1s (b), N1s (c), O1s (d), and S2p (e) of JP/SB@4:1

Table 1 Element contents (%) before and after MB, CV, and MG adsorption on JP/SB@4:1 through XPS analysis

Adsorbent	Atomic %			
	C1s	N1s	O1s	S2p
JP/SB@4:1	76.42	0.81	22.77	0
JP/SB@4:1/MB	76.13	1.67	21.85	0.35
JP/SB@4:1/MG	78.16	1.76	20.08	-
JP/SB@4:1/CV	76.63	1.65	21.72	-

charge (pH_{PZC}) of JP/SB@4:1. The pH_{PZC} of JP/SB@4:1 adsorbent was 6.7. This indicates that JP/SB@4:1 surface was positively charged when the $pH < 6.7$ due to the reaction of hydrogen ions with surface active functional groups, and was negatively charged when the $pH > 6.7$ [38]. Therefore, the maximum adsorption capacities of MB (159 mg/g), MG (156 mg/g), and CV (190.9 mg/g) were observed at pH 6.6 and 7.6, and 8.3, respectively. Similar trend was reported by Wu et al. [39] for the adsorption of MB dye using polyethyleneimine modified magnetic porous biochar. Therefore, the

pH values 6.6, 7.6, and 8.3 for MB, MG, and CV dyes were chosen as optimal pH values for the adsorption experiments.

3.2.2 Effect of contact time at various concentrations

The influence of contact time on the adsorption of cationic dyes (MB, CV, and MG) at varied C_0 : 20–100 mg/L onto JP/SB@4:1 was studied. It has been observed that the adsorption of MB, MG, and CV dyes at C_0 : 20 mg/L on JP/SB@4:1 during the initial contact time of 30 min sharply increased to 87.8 mg/g (Fig. S2a), 58.7 mg/g (Fig. S2b), and 87.8 mg/g (Fig. S2c), respectively. A sharp increase during initial 30 min was due to the availability of a large number of active adsorption sites on JP/SB@4:1 surface. Thereafter, slows down, reaching equilibrium in 480 min. The equilibrium uptake capacities of dye on JP/SB@4:1 at C_0 : 20, 60, and 100 mg/L were 147.9, 209.3, and 252.4 mg/g for MB; 149.3, 465, and 629.7 mg/g for MG; and 148, 213.9, and 233.7 mg/g for CV, respectively. Overall, the observed equilibration time for dye adsorption at varied concentrations was 480 min. However, for MB and CV adsorption at C_0 :

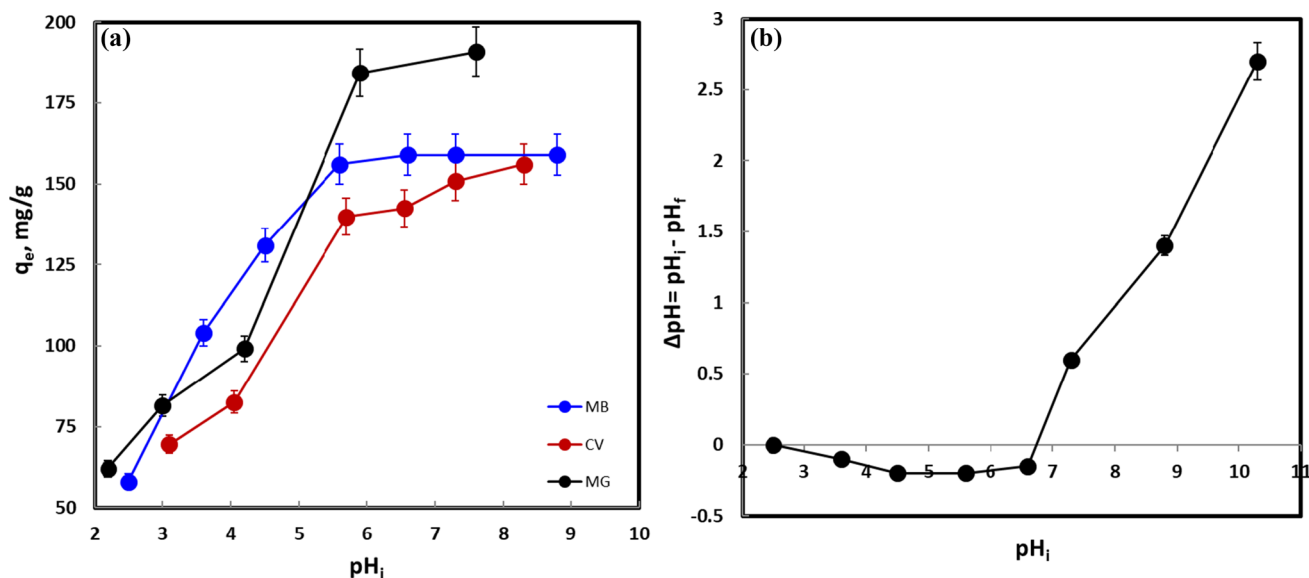


Fig. 3 pH plot for dyes adsorption on JP/SB@4:1 (a), and point of zero charge (pH_{PZC}) plot of JP/SB@4:1 (b)

100 mg/L, the equilibration time was 360 min. As illustrated in Fig. S2 (a–c), the adsorption uptake of MG on JP/SB@4:1 at varied concentrations was comparatively higher than MB and CV dyes. This may be due to the difference in the structure of each dye in terms of functional groups and molecular size. The large molecule of CV may hinder its binding to the JP/SB@4:1 surface. For MB adsorption, the positively charged sulfur ions of MB can bind with negative charge carboxyl groups present over JP/SB@4:1 surface. Thus, MB molecules occupy larger areas over the JP/SB@4:1 surface. This results in hindering the binding of additional MB molecules and thereby restricting MB adsorption over JP/SB@4:1 surface [40].

3.2.3 Effect of initial dyes concentration and temperature

The effect of initial dyes concentration on the adsorption process was investigated in temperature range: 25–55 °C. It is clear that the adsorption capacities of MB, MG, and CV dyes on JP/SB@4:1 at 25 °C were increased with increase in dyes concentrations from 20 to 100 mg/L as illustrated in Fig. S3 (a–c). At 20 mg/L, the adsorption capacities of MB, MG, and CV dyes on JP/SB@4:1 were found to be 114.9, 159.4, and 107.9 mg/g, respectively. The increase in initial concentrations of MB, MG, and CV dyes to 100 mg/L results a 115.75, 295.98, and 107.04%, increase in their adsorption capacities to maximum values of 247.9, 631.2, and 223.4 mg/g, respectively. This increase in adsorption capacities may be due to the high driving force for mass transfer [41]. Besides, the MB, MG, and CV dyes uptakes were increased with rise in temperature from 25 to 55 °C at varied concentrations. For increase in temperature from 25 to 55 °C, the adsorption capacities have

increased by 33.24, 10.72, and 10.19%, to maximum values of 153.1, 176.5, and 118.9 mg/g for MB, MG, and CV dyes, respectively at 20 mg/L, indicating that the adsorption process was endothermic in nature. This may be due to the development of new adsorption active sites over JP/SB@4:1 adsorbent surface formed by the breakage of internal bonds present over JP/SB@4:1 surface at high temperature [42]. This also results in enhanced diffusion of MB, MG, and CV molecules, reinforcing their transport into the pores of the JP/SB@4:1 adsorbent [43]. Similar adsorption behavior was observed for MB adsorption on maleylated modified hydrochar [16], and magnetic composite of coffee husk hydrochar [26].

3.3 Adsorption modeling

3.3.1 Kinetic modeling

Non-linear pseudo-first-order (PFO) [44] and pseudo-second-order (PSO) [45] kinetic models were applied to describe the dye adsorption kinetics data over JP/SB@4:1 at varied C_0 values. The non-linear PFO and PSO kinetic model equations are presented by Eqs. 4 and 5, respectively as:

$$q_t = q_e(1 - e^{-k_1 t}) \quad (4)$$

$$q_t = \frac{q_e^2 k_2 t}{1 + q_e k_2 t} \quad (5)$$

where k_1 and k_2 represent the first-order (1/min) and second-order rate (g/mg-min) constants, respectively.

The fitting of data for MB, MG, and CV adsorption onto JP/SB@4:1 were shown in Fig. S2 (a, b, and c) and kinetic

parameters were given in Table 2. It was observed that the regression coefficient (R^2) values for PSO model at varied C_o : 20–100 mg/L were comparatively higher than R^2 values for PFO model. In addition, the experimental adsorption capacity ($q_{e,exp}$) and calculated adsorption capacity ($q_{e,cal.}$) values for PSO model were nearer supporting the applicability of the PSO model for MB, MG, and CV adsorption on JP/SB@4:1. The fitting of PSO model to experimental data affirmed the adsorption of dyes on JP/SB@4:1 occurred through chemisorption mechanism which involves electron sharing or hydrogen bonding [47] Similar results were reported for MB and CV adsorption on $TiO_2@AS$ [45], and N-ACG: OOC – 3 [46], respectively.

3.3.2 Isotherm modeling

The MB, MG, and CV adsorption data on JP/SB@4:1 was modeled by non-linear Langmuir (LIM) [47] and Freundlich (FIM) [48] isotherm models. The non-linear LIM and FIM are given by Eqs. 6 and 7, respectively as:

$$q_e = \frac{q_m K_L C_e}{1 + K_L C_e} \tag{6}$$

$$R_L = \frac{1}{1 + K_L C_o} \tag{7}$$

$$q_e = K_F C_e^{1/n} \tag{8}$$

where q_m (mg/g) is the maximum monolayer capacity, K_L (L/mg) and K_F ((mg/g) (L/mg)^{1/n}) are the Langmuir and Freundlich constants, n is the adsorption intensity. R_L is a dimensionless constant termed as separation factor. The fitting of experimental data to adsorption isotherms is presented in

Fig. S3 (a–c) and Table 3 displays isotherm parameters. It was observed the isotherm fittings and R^2 values from dye adsorption data were fitted well to LIM indicating that the MB, CV, and MG adsorption onto JP/SB@4:1 followed monolayer adsorption mechanism. Based on the Langmuir equation, the q_m values for MB, CV, and MG adsorption on JP/SB@4:1 at 55 °C were found to be 326.79, 300.87, and 922.29 mg/g, respectively. These values were comparable or much higher than the recently reported values for MB, MG, and CV adsorption in the literature (Table 4) [49–56]. The obtained values for R_L parameter were between 0.2158 and 0.4378, indicating that the MB, CV, and MG dye adsorption onto JP/SB@4:1 adsorbent was favorable. The increase in the values of K_L and K_F with increased temperature from 25 to 55 °C, suggested that the adsorption of MB, CV, and MG dyes were highly favorable at 55 °C.

3.3.3 Thermodynamic modeling

The adsorption of MB, CV, and MG dyes onto JP/SB@4:1 was studied at various temperatures viz. 298, 308, 318, and 328 K and the thermodynamic parameters namely, Gibbs standard free energy change (ΔG°), standard enthalpy change (ΔH°), and standard entropy change (ΔS°) were evaluated by employing Eqs. 9, and 10 respectively as:

$$\Delta G^\circ = -RT \ln K_c \tag{9}$$

$$\ln K_c = -\frac{\Delta H^\circ}{RT} + \frac{\Delta S^\circ}{R} \tag{10}$$

where $K_c = q_e/C_e$ is the thermodynamic equilibrium constant, T is the temperature (K), and R is the gas constant. The values of ΔH° and ΔS° were estimated from the slope and

Table 2 Kinetic parameters for dye adsorption on JP/SB@4:1

C_o (mg/L)	$q_{e,exp}$ (mg/g)	Non-linear kinetic models					
		PFO			PSO		
		$q_{e,cal.}$ (mg/g)	k_1 (1/min)	R^2	$q_{e,cal.}$ (mg/g)	k_2 (g/mg-min)	R^2
MB							
20	147.99	137.00	0.03654	0.73955	146.08	0.00041	0.90445
60	209.26	196.51	0.06445	0.86793	209.08	0.00049	0.98641
100	252.39	242.52	0.0536	0.84793	256.46	0.00036	0.96641
CV							
20	100.44	89.91	0.01376	0.89592	103.77	0.00015	0.95210
60	213.86	202.65	0.02053	0.91429	223.61	0.00012	0.97245
100	233.71	227.38	0.02099	0.96106	250.85	0.00011	0.98998
MG							
20	149.33	142.49	0.01576	0.93027	160.85	0.00012	0.96526
60	465.06	431.07	0.04788	0.65260	456.29	0.00018	0.87628
100	629.69	587.47	0.05956	0.79192	624.81	0.00015	0.95741

Table 3 Isotherm parameters for dye adsorption on JP/SB@4:1

Temperature (K)	Non-linear isotherm models						
	LIM				FIM		
	q_m (mg/g)	K_L (L/mg)	R_L	R^2	K_F (mg/g)(L/mg) ^{1/n}	n	R^2
MB							
298	298.33	0.08440	0.3720	0.98904	73.110	3.343	0.95584
308	300.99	0.11683	0.2997	0.99309	91.834	3.870	0.96046
318	317.78	0.15003	0.2499	0.99744	107.93	4.139	0.97232
328	326.79	0.18165	0.2158	0.99916	118.32	4.300	0.9837
CV							
298	269.99	0.07657	0.3950	0.99387	62.367	3.240	0.96989
308	279.29	0.07309	0.4062	0.99614	61.125	3.124	0.97447
318	285.73	0.07576	0.3975	0.99507	64.075	3.164	0.97217
328	300.87	0.07613	0.3964	0.99773	64.860	3.054	0.98889
MG							
298	850.04	0.06419	0.4378	0.99085	108.50	1.981	0.96203
308	851.27	0.08411	0.3728	0.99645	130.03	2.148	0.96876
318	879.95	0.10613	0.3202	0.99864	150.71	2.310	0.97318
328	922.29	0.12350	0.2882	0.99745	166.59	2.400	0.96512

intercept of the plots of $\ln K_c$ versus $1/T$ (Fig. S4 a–c). The thermodynamic parameters of MB, CV, and MB adsorption on JP/SB@4:1 adsorbent were summarized in Table 5. The negative values of ΔG° at various temperatures indicate that the MB, CV, and MG dye adsorption onto JP/SB@4:1 was thermodynamically favorable and spontaneous process. Besides, these values were increased with the increasing

temperature, indicating a better adsorption performance at a higher temperature. The adsorption process was endothermic as the ΔH° values were positive. The ΔH° values for MB, CV, and MG dyes at C_0 : 20 mg/L were 24.30, 5.86, and 18.27 kJ/mol, respectively. These values were < 40 kJ/mol, indicating that the adsorption process was in physical adsorption range.

Table 4 Comparison of MB, CV, and MG adsorption performance on JP/SB@4:1 with different adsorbents

Adsorbent	Adsorbate	Experimental conditions	Kinetic/isotherm models	q_m (mg/g)	Reference
Jackfruit leaf powder (JLP)	CV	C_0 : 20–100 mg/L; T: 295 K; pH:7;m:1.0 g; t:120 min	PSO/LIM	43.39	[49]
γ -alumina	MB/CV	C_0 : 20–400 mg/L; T: 303 K; m: PFO (MB), PSO (CV)/LIM 0.2 g; pH: 9; t: 30 min		57.81/31.92	[50]
T. asperellum autoclaved biomass	MG/CV	C_0 : 10–50 mg/L; T: 303 K; m: PSO/(LIM- FIM) 1.0 g; pH: 10; t: 80 min -MG, 60 min -CV		52.63/62.50	[51]
Tapioca peel (S@TP) biochar	MG	C_0 : 25–150 mg/L; m: 0.1 g; pH: FIM/PSO 8; t: 120 min		30.18	[52]
Banana stem based activated carbon	MB	C_0 : 25–200 mg/L; T: 298 K; m: PSO/FIM 0.2 g; pH: 7; t: 90 min		101.01	[53]
<i>Platanus orientalis</i> leaves	MB	C_0 : 20–180 mg/L; T: 333 K; pH: 12; t: 70 min	PSO/LIM	114.94	[54]
Grapefruit peel	CV	C_0 : 25–100 mg/L; T:298 K pH:6; pH: 7; m:1.0 g; t: 60 min	PSO/LIM	249.68	[55]
Oxone treated HC	MB	C_0 : 100–150 mg/L; T:303 K pH:7; pH: 7; m:0.05 g; t: 240 min	PSO/LIM	86.70	[56]
JP/SB@4:1	MB/CV/MG	C_0 : 20–100 mg/L; T: 328 K; pH: 6.6-MB, 7.6-MG, and 8.3-CV; m: 0.005 g; t: 360 min	LIM/PSO	326.79/300.87/922.29	This study

Table 5 Thermodynamic parameters for MB, CV, and MG adsorption on JP/SB@4:1

C_o (mg/L)	Thermodynamic parameters						
	ΔH° (kJ/mol)	ΔS° (J/mol-K)	$(-)\Delta G^\circ$ (kJ/mol)				
			298 K	308 K	318 K	328 K	
MB							
20	24.30	103.16	6.45	7.41	8.57	9.50	
40	12.17	59.60	5.55	6.22	6.81	7.33	
60	8.19	43.17	4.68	5.06	5.61	5.94	
CV							
20	5.86	39.86	6.09	6.33	6.69	7.32	
40	2.98	26.67	4.96	5.21	5.49	5.76	
60	2.41	22.22	4.21	4.41	4.69	4.87	
MG							
20	18.27	92.10	9.09	10.11	11.22	11.77	
40	12.57	72.54	9.02	9.81	10.45	11.22	
60	9.62	61.32	8.68	9.23	9.82	10.54	

3.4 Comparative performance of JP/SB@4:1 with other adsorbents

The maximum adsorption capacities of JP/SB@4:1 toward MB, CV, and MG were 326.79, 300.87, and 922.29 mg/g, respectively at 55 °C, which was higher than that of the hydrochars derived from other biomass wastes displayed in Table 4 [56–63], Comparatively better adsorption

performance exhibited by JP/SB@4:1 than other hydrochars might be due to the JP was blended with SB (in varied mass ratio) during Co-HTC which led to improving the physico-chemical properties of hydrochar for the removal of MB, CV, and MG dyes from aqueous solutions. However, the suitability of potential adsorbent is assessment in term of efficiency, availability, and cost-effectiveness. In comparison, JP/SB@4:1 proved to be an effective and economical

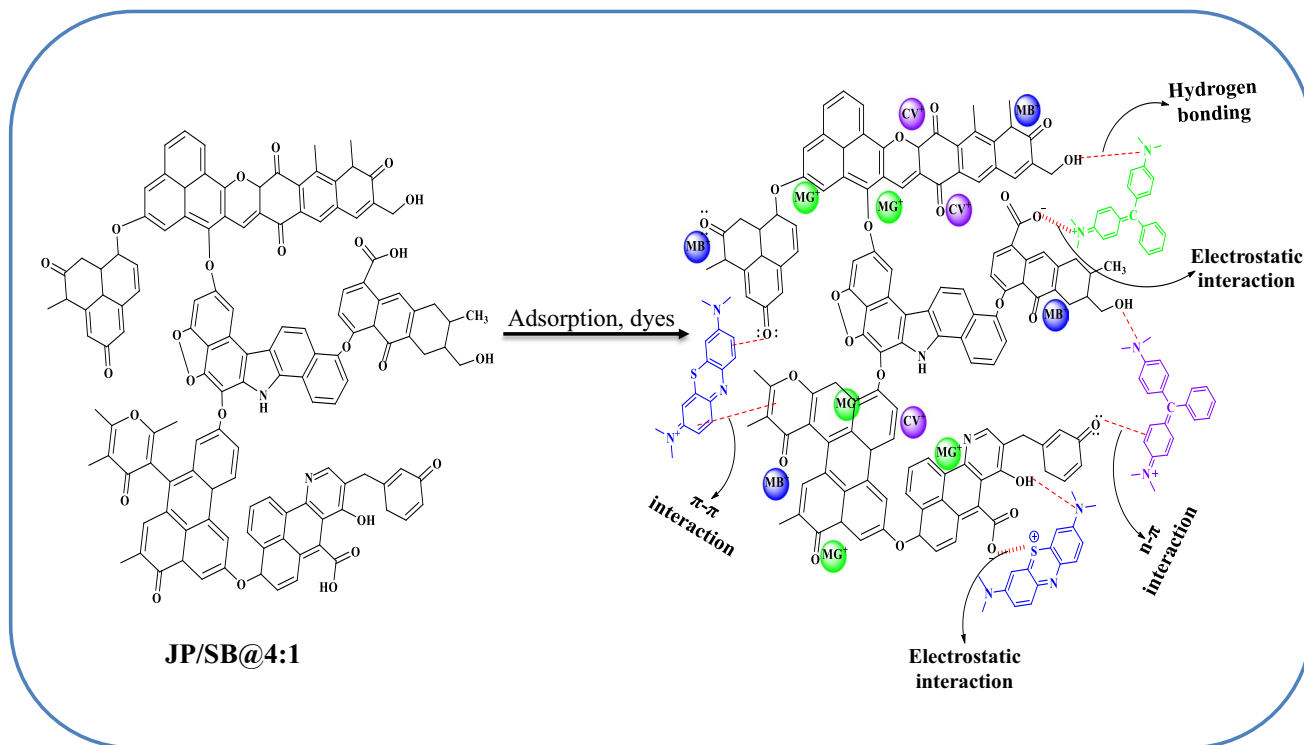


Fig. 4 Schematic representation of dyes adsorption mechanism on JF/SB@4:1

method for the removal of MB, CV, and MG from contaminated water as compared to other adsorbents.

3.5 Dye adsorption mechanism

Besides adsorption isotherm and kinetic modeling, the adsorption mechanism of dyes on JP/SB@4:1 was investigated through FTIR, and XPS analysis. According to the results of FTIR, C=O, COOH, and OH functional groups participated during the adsorption of MB, CV, and MG on JP/SB@4:1. In detail, a peak at 3441 cm^{-1} was decreased in intensity after MG and MB adsorption, while increase in peak intensity after CV adsorption was observed. This suggests that OH bond which present on the JP/SB@4:1 surface undergoes hydrogen bonding with nitrogen atoms present in dyes molecules [23]. In addition, a peak 1369 cm^{-1} was increased in intensity and shifted to lower wavenumbers (1357 , 1324 , and 1365 cm^{-1}) after CV, MB, and MG adsorption, respectively. These shifts in wavenumbers were due to the interaction of carboxyl group present over JP/SB@4:1 surface with $-\text{N}(\text{CH}_3)_2^+$ group of dye molecules by electrostatic interaction [23]. A peak at 1606 cm^{-1} was increased and shifted to 1582 , 1594 , and 1582 cm^{-1} owing to the interaction of aromatic rings with JP/SB@4:1. Beside new peaks were appeared after CV, MG, and MB adsorption which proves the successful adsorption of dyes on the JP/SB@4:1 surface [16]. According to XPS analysis, the contents of N1s in JP/SB@4:1 (0.81%) were increased to 1.67%, 1.65%, and 1.69% after the adsorption of MB, CV, and MG onto JP/SB@4:1, respectively (Table 1). In addition, a new peak appeared at 164.55 eV attributed to the S2p in MB molecules (Fig. 2e). On a whole, the mechanism that might happen during the adsorption of MB, CV, and MG dyes are presented in Fig. 4. According to thermodynamic results, a lower value of ΔH° indicates that the adsorption mechanism is a physical process. Therefore, the possible mechanism of MB, CV, and MG dye adsorption onto JP/SB@4:1 includes electrostatic interaction, hydrogen bonding, and π - π/n - π interactions.

4 Conclusions

Current study reported the blending of food wastes (JF and SB) powders in 4:1 weight ratio and thereafter Co-HTC carbonizing it to develop JP/SB@4:1. JP/SB@4:1 was characterized through FTIR, XPS, SEM, EDX, and XRD and tested for the removal of MB, CV, MG dyes from aqueous environment. Results exhibits excellent adsorption performance JP/SB@4:1 toward MB, CV, and MG molecules. The equilibration time during dye adsorption was reached in 360 min at pH values 6.6 for MB, 7.6 for MG, and 8.3 for CV and temperature 328 K. The PSO and LIM were

the best fitted models to the adsorption data. The q_m values of 326.79 and 300.87, and 922.29 mg/g for MB, CV, and MG, respectively, were observed at 328 K. Thermodynamic parameters exhibited that the adsorption process is feasible, spontaneous, and endothermic. The dye adsorption mechanism involves electrostatic interaction, hydrogen bond interaction, and π - π/n - π interaction. Overall, results indicated that JP/SB@4:1 is a promising adsorbent in the removal of dyes from aqueous solutions.

Supplementary Information The online version contains supplementary material available at <https://doi.org/10.1007/s13399-022-03711-7>.

Acknowledgements Moonis Ali Khan acknowledges the financial support through Researchers Supporting Project number (RSP2023R345), King Saud University, Riyadh, Saudi Arabia.

Author contribution Conceptualization: Moonis Ali Khan; investigation: Saikh Mohammad Wabaidur; data curation: Saikh Mohammad Wabaidur, Ayoub Abdullah Alqadami, Moonis Ali Khan; writing—original draft: Ayoub Abdullah Alqadami; formal analysis: Moonis Ali Khan; validation: Moonis Ali Khan, Byoung-Hun Jeon; writing—reviewing and editing: Moonis Ali Khan, Byoung-Hun Jeon.

Funding Funding provided by the financial support through Researchers Supporting Project number (RSP2023R345), King Saud University, Riyadh, Saudi Arabia.

Data availability All data generated or analyzed during this study are included in this manuscript.

Declarations

Ethical approval Not applicable.

Competing interests The authors declare no competing interests.

References

- Ahmad AA, Ahmad MA, Yahaya NKEM, Karim J (2021) Adsorption of malachite green by activated carbon derived from gasified Hevea brasiliensis root. *Arabian J Chem* 14:103104. <https://doi.org/10.1016/j.arabjc.2021.103104>
- Ma ZW, Zhang KN, Zou ZJ, Lü QF (2021) High specific area activated carbon derived from chitosan hydrogel coated tea saponin: one-step preparation and efficient removal of methylene blue. *J Environ Chem Eng* 9:105251. <https://doi.org/10.1016/j.jece.2021.105251>
- Tan G, Li X, Xiao D (2020) Adsorption of methylene blue onto porous carbon materials prepared from Na₂EDTA. *New J Chem* 44:4071–4080. <https://doi.org/10.1039/C9NJ06154A>
- Chen D, Zhang H, Yang K, Wang H (2016) Functionalization of 4-aminothiophenol and 3-aminopropyltriethoxysilane with graphene oxide for potential dye and copper removal. *J Hazard Mater* 310:179–187. <https://doi.org/10.1016/j.jhazmat.2016.02.040>
- Minghua Z, Xiumin F, Rovetta A, Qichang H, Vicentini F, Bingkai L, Giusti A, Yi L (2009) Municipal solid waste management in Pudong New Area, China. *Waste Manag* 29:1227–1233. <https://doi.org/10.1016/j.wasman.2008.07.016>

6. Nguyen MV, Lee BK (2015) Removal of dimethyl sulfide from aqueous solution using cost-effective modified chicken manure biochar produced from slow pyrolysis. *Sustain* 7:15057–15072. <https://doi.org/10.3390/su71115057>
7. Sharma HB, Sarmah AK, Dubey B (2020) Hydrothermal carbonization of renewable waste biomass for solid biofuel production: a discussion on process mechanism, the influence of process parameters, environmental performance and fuel properties of hydrochar. *Renew Sustain Energy Rev* 123:109761. <https://doi.org/10.1016/j.rser.2020.109761>
8. Gupta D, Mahajani SM, Garg A (2020) Investigation on hydrochar and macromolecules recovery opportunities from food waste after hydrothermal carbonization. *Sci Total Environ* 749:142294. <https://doi.org/10.1016/j.scitotenv.2020.142294>
9. Kang S, Li X, Fan J, Chang J (2012) Characterization of hydrochars produced by hydrothermal carbonization of lignin, cellulose, D-xylose, and wood meal. *Ind Eng Chem Res* 51:9023–9031
10. Elsayed I, Madduri S, El-Giar EM, Hassan EB (2022) Effective removal of anionic dyes from aqueous solutions by novel poly-ethylenimine-ozone oxidized hydrochar (PEI-OzHC) adsorbent. *Arabian J Chem* 15:103757. <https://doi.org/10.1016/j.arabj.2022.103757>
11. Tran TH, Le AH, Pham TH, Nguyen DT, Chang SW, Chung WJ, Nguyen DD (2020) Adsorption isotherms and kinetic modeling of methylene blue dye onto a carbonaceous hydrochar adsorbent derived from coffee husk waste. *Sci Total Environ* 725:138325. <https://doi.org/10.1016/j.scitotenv.2020.138325>
12. Li Y, Meas A, Shan S, Yang R, Gai X (2016) Production and optimization of bamboo hydrochars for adsorption of Congo red and 2-naphthol. *Biores Technol* 207:379–386. <https://doi.org/10.1016/j.biortech.2016.02.012>
13. Islam MT, Chambers C, Toufiq Reza M (2022) Effects of process liquid recirculation on material properties of hydrochar and corresponding adsorption of cationic dye. *J Anal Appl Pyrol* 161:105418. <https://doi.org/10.1016/j.jaap.2021.105418>
14. Haris M, Khan MW, Paz-Ferreiro J, Mahmood N, Eshtiaghi N (2022) Synthesis of functional hydrochar from olive waste for simultaneous removal of azo and non-azo dyes from water. *Chem Eng J Adv* 9:100233. <https://doi.org/10.1016/j.cej.2021.100233>
15. Tu W, Liu Y, Xie Z, Chen M, Ma L, Du G, Zhu M (2021) A novel activation-hydrochar via hydrothermal carbonization and KOH activation of sewage sludge and coconut shell for biomass wastes: preparation, characterization and adsorption properties. *J Colloid Interf Sci* 593:390–407. <https://doi.org/10.1016/j.jcis.2021.02.133>
16. Li B, Guo J, Lv K, Fan J (2019) Adsorption of methylene blue and Cd(II) onto maleylated modified hydrochar from water. *Environ Poll* 254:113014. <https://doi.org/10.1016/j.envpol.2019.113014>
17. Foo KY, Hameed BH (2012) Potential of jackfruit peel as precursor for activated carbon prepared by microwave induced NaOH activation. *Biores Technol* 112:143–150. <https://doi.org/10.1016/j.biortech.2012.01.178>
18. Sundarraj AA, Ranganathan TV (2018) Extraction and characterization of cellulose from jackfruit peel. *J Exp Biol Agri Sci* 6:414–424
19. Ahmad S, Wong YC, Veloo KV (2018) Sugarcane bagasse powder as biosorbent for reactive red 120 removals from aqueous solution. *IOP Conf Series: Earth Environ Sci* 140:012027. <https://doi.org/10.1088/1755-1315/140/1/012027>
20. Tahir H, Sultan M, Akhtar N, Hameed U, Abid T (2016) Application of natural and modified sugar cane bagasse for the removal of dye from aqueous solution. *J Saudi Chem Soc* 20:S115–S121. <https://doi.org/10.1016/j.jscs.2012.09.007>
21. Khan MA, Hameed BH, Siddiqui MR, Allothman ZA, Alshoaimi IH (2022) Physicochemical, structural and combustion analyses to estimate the solid fuel efficacy of hydrochar developed by co-hydrothermal carbonization of food and municipal wastes. *Biomass ConverBioref* (Accepted) <https://doi.org/10.1007/s13399-022-02875-6>
22. Parra-Marfil A, Ocampo-Pérez R, Collins-Martínez VH, Flores-Vélez LM, Gonzalez-García R, Medellín-Castillo NA, Labrada-Delgado GJ (2020) Synthesis and characterization of hydrochar from industrial Capsicum annum seeds and its application for the adsorptive removal of methylene blue from water. *Environ Res* 184:109334. <https://doi.org/10.1016/j.envres.2020.109334>
23. Li HZ, Zhang YN, Guo JZ, Lv JQ, Huan WW, Li B (2021) Preparation of hydrochar with high adsorption performance for methylene blue by co-hydrothermal carbonization of polyvinyl chloride and bamboo. *Biores Technol* 337:125442. <https://doi.org/10.1016/j.biortech.2021.125442>
24. Islam MA, Ahmed MJ, Khanday WA, Asif M, Hameed BH (2017) Mesoporous activated carbon prepared from NaOH activation of rattan (*Lacosperma secundiflorum*) hydrochar for methylene blue removal. *Ecotoxicol Environ Saf* 138:279–285. <https://doi.org/10.1016/j.ecoenv.2017.01.010>
25. Li F, Zimmerman AR, Hu X, Yu Z, Huang J, Gao B (2020) One-pot synthesis and characterization of engineered hydrochar by hydrothermal carbonization of biomass with ZnCl₂. *Chemosphere* 254:126866. <https://doi.org/10.1016/j.chemosphere.2020.126866>
26. Krishna Murthy TP, Gowrishankar BS, Krishna RH, Chandraprabha MN, Mathew BB (2020) Magnetic modification of coffee husk hydrochar for adsorptive removal of methylene blue: isotherms, kinetics and thermodynamic studies. *Environ Chem Ecotoxicol* 2:205–212. <https://doi.org/10.1016/j.enceco.2020.10.002>
27. Liu JL, Qian WC, Guo JZ, Shen Y, Li B (2021) Selective removal of anionic and cationic dyes by magnetic Fe₃O₄-loaded amine-modified hydrochar. *Biores Technol* 320:124374. <https://doi.org/10.1016/j.biortech.2020.124374>
28. Saqib NU, Baroutian S, Sarmah AK (2018) Physicochemical, structural and combustion characterization of food waste hydrochar obtained by hydrothermal carbonization. *Biores Technol* 266:357–363. <https://doi.org/10.1016/j.biortech.2018.06.112>
29. Wada M, Heux L, Sugiyama J (2004) Polymorphism of cellulose I family: reinvestigation of cellulose IVI. *Biomacromol* 5:1385–1391. <https://doi.org/10.1021/bm0345357>
30. Nizamuddin S, Siddiqui MTH, Baloch HA, Mubarak NM, Griffin G, Madapusi S, Tanksale A (2018) Upgradation of chemical, fuel, thermal, and structural properties of rice husk through microwave-assisted hydrothermal carbonization. *Environ Sci Poll Res* 25:17529–17539. <https://doi.org/10.1007/s11356-018-1876-7>
31. Chen W, Yu H, Liu Y, Chen P, Zhang M, Hai Y (2011) Individualization of cellulose nanofibers from wood using high-intensity ultrasonication combined with chemical pretreatments. *Carb Poly* 83:1804–1811. <https://doi.org/10.1016/j.carbpoly.2010.10.040>
32. Li Y, Zimmerman AR, He F, Chen J, Han L, Chen H, Hu X, Gao B (2020) Solvent-free synthesis of magnetic biochar and activated carbon through ball-mill extrusion with Fe₃O₄ nanoparticles for enhancing adsorption of methylene blue. *Sci Total Environ* 722:137972. <https://doi.org/10.1016/j.scitotenv.2020.137972>
33. Hou Y, Liang Y, Hu H, Tao Y, Zhou J, Cai J (2021) Facile preparation of multi-porous biochar from lotus biomass for methyl orange removal: kinetics, isotherms, and regeneration studies. *Biores Technol* 329:124877. <https://doi.org/10.1016/j.biortech.2021.124877>
34. Cai T, Liu X, Zhang J, Tie B, Lei M, Wei X, Peng O, Du H (2021) Silicate-modified oiltea camellia shell-derived biochar: a novel and cost-effective sorbent for cadmium removal. *J Clean Prod* 281:125390. <https://doi.org/10.1016/j.jclepro.2020.125390>
35. Shi G, Ruan C, He S, Pan H, Chen G, Ma Y, Dai H, Chen X, Yang X (2021) Zr-based MOF @ carboxymethylated filter paper: insight into construction and methylene blue removal mechanism.

- Colloids Surf A 613:126053. <https://doi.org/10.1016/j.colsurfa.2020.126053>
36. De Marco C, Mauler RS, Daitx TS, Krindges I, Cemin A, Bonetto LR, Crespo JS, Guégan R, Carli LN, Giovanela M (2020) Removal of malachite green dye from aqueous solutions by a magnetic adsorbent. *Sep Sci Technol* 55:1089–1101. <https://doi.org/10.1080/01496395.2019.1585455>
37. Ekmen E, Bilici M, Turan E, Tamer U, Zengin A (2020) Surface molecularly-imprinted magnetic nanoparticles coupled with SERS sensing platform for selective detection of malachite green. *Sensors Actuators B* 325:128787. <https://doi.org/10.1016/j.snb.2020.128787>
38. Ahmad R, Ansari K (2021) Comparative study for adsorption of congo red and methylene blue dye on chitosan modified hybrid nanocomposite. *Process Biochem* 108:90–102. <https://doi.org/10.1016/j.procbio.2021.05.013>
39. Wu Z, Wang X, Yao J, Zhan S, Li H, Zhang J, Qiu Z (2021) Synthesis of polyethyleneimine modified CoFe₂O₄-loaded porous biochar for selective adsorption properties towards dyes and exploration of interaction mechanisms. *Sep Purif Technol* 277:119474. <https://doi.org/10.1016/j.seppur.2021.119474>
40. Geçgel Ü, Üner O, Gökara G, Bayrak Y (2016) Adsorption of cationic dyes on activated carbon obtained from waste *Elaeagnus* stone. *Adsorp Sci Technol* 34:512–525. <https://doi.org/10.1177/02636174166669727>
41. Tharaneedhar V, Kumar PS, Saravanan A, Ravikumar C, Jaikumar V (2017) Prediction and interpretation of adsorption parameters for the sequestration of methylene blue dye from aqueous solution using microwave assisted corncob activated carbon. *Sustain Mater Technol* 11:1–11
42. Nirmaladevi S, Palanisamy N (2020) A comparative study of the removal of cationic and anionic dyes from aqueous solutions using biochar as an adsorbent. *Desal Water Treat* 175:282–292. <https://doi.org/10.5004/dwt.2020.24906>
43. Doan VD, Tran TKN, Nguyen AT, Tran VA, Nguyen TD, Le VT (2021) Comparative study on adsorption of cationic and anionic dyes by nanomagnetite supported on biochar derived from *Eichhornia crassipes* and *Phragmites australis* stems. *Environ Nanotechnol Monitor Manag* 16:100569. <https://doi.org/10.1016/j.enmm.2021.100569>
44. Lagergren S (1898) About the theory of so-called adsorption of soluble substances. *Handlingar* 24:1–39
45. Geng Y, Zhang J, Zhou J, Lei J (2018) Study on adsorption of methylene blue by a novel composite material of TiO₂ and alum sludge. *RSC Adv* 8:32799–32807. <https://doi.org/10.1039/C8RA05946B>
46. Alshareef SA, Alqadami AA, Khan MA, Alanazi HS, Siddiqui MR, Jeon BH (2022) Simultaneous co-hydrothermal carbonization and chemical activation of food wastes to develop hydrochar for aquatic environmental remediation. *Biores Technol* 347:126363. <https://doi.org/10.1016/j.biortech.2021.126363>
47. Wallis A, Dollard MF (2008) Local and global factors in work stress - the Australian dairy farming exemplar, *Scandinavian J Work, Environ Health, Suppl* 66–74.
48. Über die Adsorption in Lösungen (1907) *Z Phys Chem* 57U:385. <https://doi.org/10.1515/zpch-1907-5723>
49. Saha PD, Chakraborty S, Chowdhury S (2012) Batch and continuous (fixed-bed column) biosorption of crystal violet by *Artocarpus heterophyllus* (jackfruit) leaf powder. *Colloids Surf B* 92:262–270. <https://doi.org/10.1016/j.colsurfb.2011.11.057>
50. Fernandes EP, Silva TS, Carvalho CM, Selvasembian R, Chaukura N, Oliveira LMTM, Meneghetti SMP, Meili L (2021) Efficient adsorption of dyes by γ -alumina synthesized from aluminum wastes: kinetics, isotherms, thermodynamics and toxicity assessment. *J Environ Chem Eng* 9:106198. <https://doi.org/10.1016/j.jece.2021.106198>
51. Shanmugam S, Karthik K, Veerabagu U, Hari A, Swaminathan K, Al-Kheraif AA, Whangchai K (2021) Bi-model cationic dye adsorption by native and surface-modified *Trichoderma asperellum* BPL MBT1 biomass: from fermentation waste to value-added biosorbent. *Chemosphere* 277:130311. <https://doi.org/10.1016/j.chemosphere.2021.130311>
52. Vigneshwaran S, Sirajudheen P, Karthikeyan P, Meenakshi S (2021) Fabrication of sulfur-doped biochar derived from tapioca peel waste with superior adsorption performance for the removal of malachite green and Rhodamine B dyes. *Surf Interf* 23:100920. <https://doi.org/10.1016/j.surfin.2020.100920>
53. Misran E, Bani O, Situmeang EM, Purba AS (2022) Banana stem based activated carbon as a low-cost adsorbent for methylene blue removal: isotherm, kinetics, and reusability. *Alexandria Eng J* 61(2022):1946–1955. <https://doi.org/10.1016/j.aej.2021.07.022>
54. Peydayesh M, Rahbar-Kelishami A (2015) Adsorption of methylene blue onto *Platanus orientalis* leaf powder: kinetic, equilibrium and thermodynamic studies. *J Ind Eng Chem* 21:1014–1019. <https://doi.org/10.1016/j.jiec.2014.05.010>
55. Saeed A, Sharif M, Iqbal M (2010) Application potential of grapefruit peel as dye sorbent: kinetics, equilibrium and mechanism of crystal violet adsorption. *J Hazard Mater* 179:564–572. <https://doi.org/10.1016/j.jhazmat.2010.03.041>
56. Madduri S, Elsayed I, Hassan EB (2020) Novel oxone treated hydrochar for the removal of Pb(II) and methylene blue (MB) dye from aqueous solutions. *Chemosphere* 260:127683. <https://doi.org/10.1016/j.chemosphere.2020.127683>

Publisher's note Springer Nature remains neutral with regard to jurisdictional claims in published maps and institutional affiliations.

Springer Nature or its licensor (e.g. a society or other partner) holds exclusive rights to this article under a publishing agreement with the author(s) or other rightsholder(s); author self-archiving of the accepted manuscript version of this article is solely governed by the terms of such publishing agreement and applicable law.